International journal of COMADEM
Vol # No # (January 2017) p.##-##

COMADEM

International Journal of Condition Monitoring and Diagnostic Engineering Management

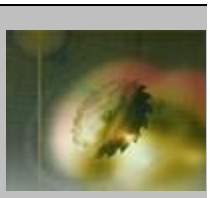

An experimental study of front surface thermal performance of domestic and commercial electric heating solutions using thermography and thermocouples

Karina Zala[a] *, Aliyu Aliyu[a], Rakesh Mishra[a], Scott Conor[b], Fiona Conor[b], Naeem Mian[a]

[a] *University of Huddersfield, Queensgate, Huddersfield, West Yorkshire HD1 3DH, England, UK*
[b] *Trust Electric Heating, Elmfield Business Park, 12, Trust House, Lotherton Way, Garforth, Leeds LS25 2JY*

∗ *Corresponding author email*: *karinazala@hotmail.com*

ABSTRACT

The UK government is developing green schemes and introducing new legislations for future housing. This is having a positive effect on the general population causing them to switch from gas to electric heating. In addition to this, new build housings are also strongly encouraged to install only electric heating systems in line with the
legislation. Electric heating is therefore becoming more popular and as there are many heating systems available in the marketplace, there is a need to analyse the performance of various heating systems. This study explores the heat map of front surface temperatures using thermography and thermocouples of commonly used heating systems. Five electric heating samples used in the commercial and domestic markets and dwellings have been investigated during this study. The purpose of this paper is to quantify and compare the heating and cooling cycles of various types of electric heating systems. It is also to identify to what extent the heating takes place for each sample. Results depicted that the Trust sample had the lowest surface temperature out of the five samples, meaning it is the safest sample to being in contact with that has been tested. Further to this, Sample B reached extremely high temperatures exceeding above 100°C surface temperature during its heating cycle. Further work is required to clarify and quantify thermal inertia of the samples.

Keywords: *electric radiator; thermography; thermocouples.*
Article history: *Received ; Published .*

1. Introduction

Electric heating is becoming more popular due to the government green schemes and planned legislations in place for new-build housing [1]–[3]. An average person in the UK is responsible for 2.6 tonnes of carbon dioxide emissions per year. A large amount of the emissions is as a result of domestic and industrial space heating. This has captured attention of the UK government, activists, and policy makers and raised the awareness of the UK public to address this issue vis-à-vis global warming. To this effect, the UK government has set out a challenging target of aiming to reduce 60% of these emissions by 2050. Given these enforcements via UK policies and legislations, there are many electric heating solutions in the market that exhibit different thermal characteristic behaviours. Efficient heating is characterised by numerous factors such as, appropriately specified radiator size for a given space, internal surface area, materials, and the geometric design features of the radiator [4] as well as the heater's safety to a building's inhabitants especially if vulnerable such as the elderly or disabled. Hence, analysing the characteristics of various heaters in the marketplace is important in understanding the status of the currently available heating solutions' characteristics for low surface temperature and hence safe operation.

2. Literature review

Before going into the details of the heaters sampled for the current study, a brief review of the space heating literature will first be carried out. Hemadri et al. [5] used infrared thermography and simulations to investigate the thermal performance of embedding pulsating heat pipe (PHP) structures in two different base plates: one of mild steel and the other of aluminium having two effective Biot numbers with natural convection and radiation heat transfer conditions on the surface. Calisir et al. [6] used thermography during their experimentation and Computational Fluid Dynamics (CFD) to study thermal performance of panel-convector-convector-panel (PCCP) radiators for different convector fin dimensions. Taheri-Garavand et al. [7] used thermography to investigate the new intelligent fault diagnosis and condition monitoring system for classification of six different fault conditions of cooling radiator using infrared thermal images. Wernik et al. [8] used CFD and thermography to study thermal analysis of a radiator under natural and forced convection. Following on from the study Asim et al. [4] carried out on the thermal characterisation of electric radiators. This paper explores five electric heating samples used in commercial and domestic environments by carrying out an experimental study using thermography. Altwieb et al. [9] numerically studied various configurations of a multi-tube heat exchanger to study its space heating characteristics. They developed semi-analytical correlations for

optimising the heater configuration. The numerical model was validated with experiments [10] and developed two new correlations based on the experimental data which they showed were to within ±15% of the experimental data. Given the previous studies reviewed above, it has been noted that a holistic approach to efficient, safe space heating, indoor air quality, and carbon emissions is needed, especially since the advent of COVID-19 [11].

One of the drawbacks of many heaters in the market is their high surface temperature, which can be a health hazard to especially children in schools and seniors in care homes. In order to minimise cases of heater surface burn mishaps, it is important that current and future electric heaters are developed to be so that these have low surface temperature (LST) and heat efficiently. LST heaters are defined as those with surface temperatures not exceeding 43ºC [12]–[14]. In order to aid the development of LSTs it is important to understand the heating characteristics of available heaters in the market, their heating cycles, and maximum surface temperatures in relation to their design and core material.

Based on this premise, five commercially available electric heaters used for commercial and domestic heating were obtained and experimentally tested in this study. This is to ascertain the closeness or otherwise to being LST or otherwise of currently sold electric heater models. Furthermore, the study quantifies and compares their heating and cooling characteristics (thermal inertia) over time using both thermal imaging for high spatial resolution which were validated with thermocouple measurements.

3. Methodology

This experimental study is aimed at understanding the thermal behaviours of various electric heating samples. Five commercially available heater models were procured for testing. The samples have been carefully selected from the domestic and commercial market space and these are:

- Trust electric radiator with a soapstone core and a power output of 1.2kW is shown in Figure 1.
- Sample A, radiator with a fire clay core and a power output of 1kW is shown in Figure 2.
- Sample B, radiator with a clay chamotte core and a power output of 1.3kW is shown in Figure 3.
- Sample C, panel Radiators with an oil-filled core and a power output of 1.5kW is shown in Figure 4.
- Sample D, panel convector heater with an electric filament core and a power output of 1.3kw is shown in Figure 5.

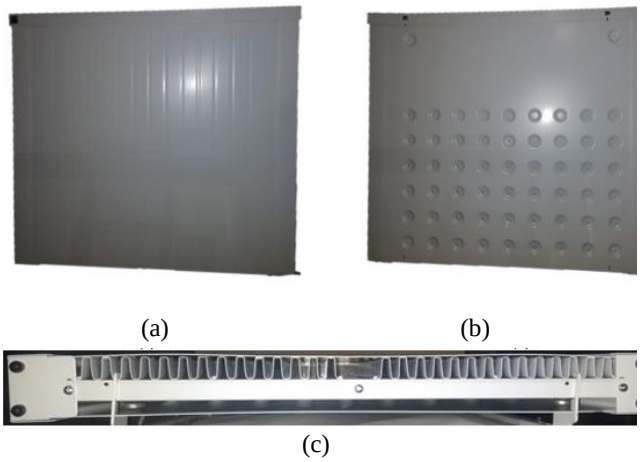

Figure 1. Trust electric radiator (a) front (b) rear surface (c) core

Figure 2: Sample A, radiator, fireclay core (a) electric radiator (b) core

Figure 3: Sample B, radiator, clay chamotte core (a) electric radiator (b) core

Figure 4. Sample C, oil-filled panel radiator

(a) (b)

Figure 5. Sample D, Electric panel heater, filament core (a) electric radiator (b) core

FLIR A655sc thermal camera [15], shown in Figure 6 (a) has been used to capture and characterise thermal behaviour of the samples. This is a self-calibrating thermal camera and senses temperature via infrared. Its resolution is 640 x 480, spectral range is 7.5–14.0μm and accuracy is ±2°C or ±2% of reading [10]. The camera had been mounted onto a tripod and necessary adjustments had been made to align the camera with respect to the sample and to avoid reflections. The experimental setup is shown in Figure 6(b). The radiator samples have been mounted on a custom-built wooden stand to mimic the effects of the back wall.

(a) (b)

Figure 6. Thermal setup (a) thermal camera; (b) setup

Thermocouples have been mounted on the radiator samples on 5 distinct positions as shown in Figure 7.

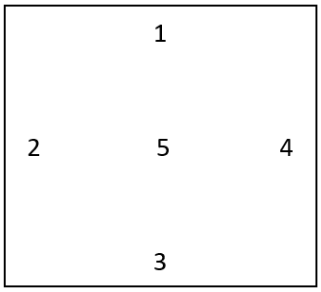

Figure 7. Thermocouple position on radiator front surface

4. Data Collection and Analysis

4.1. Validation

Figure 8 depicts the validation of the thermography data against thermocouple data of the Trust sample, which have been collected as aforementioned in Figure 7. Validating thermal image with the thermocouple sensor has depicted a maximum difference for position (1) at the top front radiator surface of 16.8%, while the minimum of 0.1%. For position (2) at the left front radiator surface, these are 7.3% and 0%. For position (3) at the bottom front radiator surface, the maximum and minimum differences are 4.8% and 0%, respectively. For position (4) at the right front radiator surface, the maximum difference is 7.1% and the minimum difference is 0.2%. For position (5) at the centre front radiator surface, these are 14.9% and 0.1%, respectively.

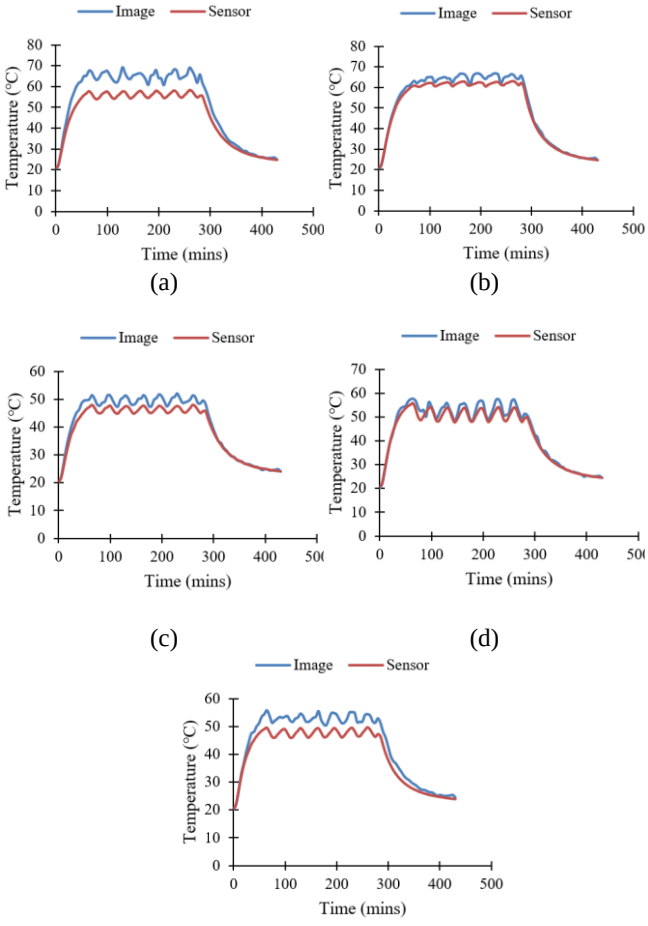

Figure 8. Validation of thermocouples against themography on front radiator surface (a) top (b) left (c) bottom (d) right and (e) centre

Figure 9 depicts the front surface validation of all five samples between thermography and thermocouples. The maximum and minimum variations between the two for the Trust sample is 13.3% and 0.3%; for the radiator A, these are 21.6% and 0%; for radiator B, these are 12.2% and 0.7%; for radiator C, these are 18.4% and 0.2%; and for radiator D, these

are 33.2% and 0.4%. Aside from the validation, it is noticed that the Trust sample predominantly depicts the lowest front surface temperature in both instances of thermography and thermocouple testing during its warm-up and steady state. It is noticed that the Trust sample and the radiator A sample are the only ones that appear to retain heat in its core to cut-off during its steady-state period. It can also be seen that radiator B exceeds 100°C on the front surface temperature, which may cause health and safety issues. Further to this, is can be seen the radiator D takes the shortest amount of time at 15 minutes to reach its steady state due to the natural of its heat source while the radiator B takes the longest time at 150 minutes.

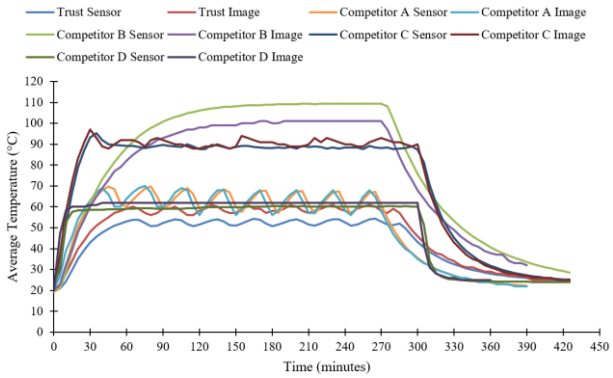

Figure 9. Front surface validation of all samples

5. Results & Discussion

5.1. Thermography Measurements

Thermography data has been presented below. Table 1 depicts the heating cycle. The temperature fields for Trust sample and Sample A both have been depicted on a scale from 20°C to 91°C; the temperature fields for Sample B is depicted on a scale from 20°C to 153°C; the temperature fields for Sample C is depicted on a scale from 20°C to 111°C; and the temperature fields for Sample D is depicted on a scale from 20°C to 124°C. The samples are on their independent scales to clearly observe and understand how each sample varies with respect to time.

For the Trust sample, which has a soapstone core and is manufactured from aluminium, it can be seen that after 15 minutes of heating, the top of the radiator heats up first. As time lapses, heat increases and propagates to either sides of the sample, then is distributed across the middle and downwards. This trend suggests that heated air is convecting into the room as the prominent regions are towards the top grill. The maximum temperature of this sample reaches 91°C and maximum average temperature this sample reaches 59°C showing higher temperature on the left side of the radiator in comparison to the right.

For sample A, which is with a fireclay core and is manufactured from mild steel, it can be seen that after 15 minutes of heating, the prominent regions are in the central bottom region. This propagates towards the top whereby the core can be seen due to the tablets emitting high heat zones. This is a dual finned sample on either side of its core, suggesting these high heated zones could be a result of blockages in the fins, restricting air flow, thus, also in turn minimimising the heat transfer [7]. The maximum temperature of this sample reaches 91°C and maximum average temperature this sample reaches 70°C showing prominent high heat distribution across the sample surface. This high heat propagating across suggests that metal is retaining the heat rather than convecting into the environment. There are relatively high levels of radiant heat being emitted in comparision to the Trust sample.

For sample B, which is with a clay chamotte core and is manufactured from mild steel, shows a high temperature region across the mid-lower sector after 15 minutes of heating. As time elapses, the mid-upper sector exhibits high temperatures, propagating towards the central region. The temperature in the lower sector continues to increase significantly during this time. At the maximum temperature, the top of the sample depicts high thermal zones. The maximum temperature this sample has exhibited is 153°C and its maximum average temperature is 101°C, depicting prominent high heat zone on the lower sector of the sample. These extreme temperatures across the sample indicate that heat is predominantly being held inside the sample rather than discharging into the environment via radiation. Although this is the predominant method observed of the heat discharging from this sample, high thermal zone observed at the top of the sample also indicates the discharge of the generated heat is also being convected into the room.

For sample C, which has an oil-filled core and is manufactured from mild steel, shows there is reasonably uniform thermal distribution across this sample. The bottom of the sample heats up first after 15 minutes of heating and continues to increase in temperature as time elapses. The maximum temperature the sample reaches in the testing period of heating cycle is 106°C and the maximum average temperature is 93°C. The uniform high temperature distribution across the panel indicates that heat is emitted into the room via radiation. This also shows the sample is holding onto the heat in itself. This again, is a result of the mild steel material used as the carcass of the sample.

For sample D, which has an electric filament core and is manufactured from steel, it can be seen that the filament heats up significantly in the first 15 minutes. This heat distributes across to it convective grills and the upper half of the sample. There a little variations on the heat distribution across the sample as time elapses. The maximum temperature exhibited towards the end of its heating cycle and 124°C and its maximum average temperature is 63°C.

Table 1. Heating Cycle Independent Analysis

Time (mins)	Thermography Data					
	Trust		Sample A, Fireclay Radiator		Sample B, Clay Chamotte Radiator	
					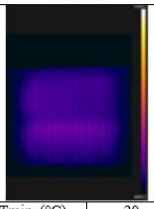	
	Tmin. (°C)	22	Tmin. (°C)	21	Tmin. (°C)	20
	Tmax. (°C)	43	Tmax. (°C)	61	Tmax. (°C)	58
15	Tave. (°C)	34	Tave. (°C)	46	Tave. (°C)	40
	Sample C, Oil-filled Panel Heater				Sample D, Electric Filament Heater	
	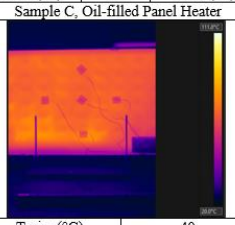				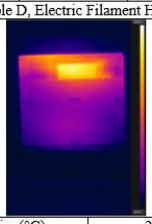	
	Tmin. (°C)	40			Tmin. (°C)	23
	Tmax. (°C)	85			Tmax. (°C)	121
	Tave. (°C)	72			Tave. (°C)	60
	Trust		Sample A, Fireclay Radiator		Sample B, Clay Chamotte Radiator	
	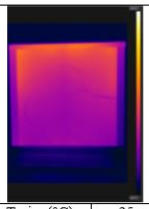		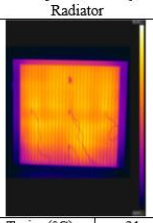		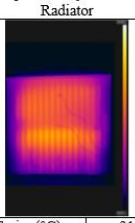	
	Tmin. (°C)	25	Tmin. (°C)	21	Tmin. (°C)	21
	Tmax. (°C)	65	Tmax. (°C)	82	Tmax. (°C)	89
30	Tave. (°C)	48	Tave. (°C)	63	Tave. (°C)	60
	Sample C, Oil-filled Panel Heater				Sample D, Electric Filament Heater	
	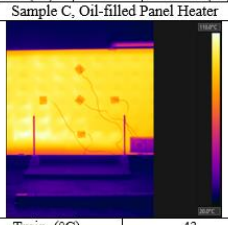				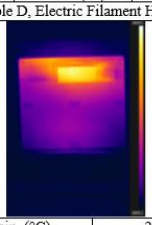	
	Tmin. (°C)	43			Tmin. (°C)	24
	Tmax. (°C)	110			Tmax. (°C)	121
	Tave. (°C)	97			Tave. (°C)	61
	Trust		Sample A, Fireclay Radiator		Sample B, Clay Chamotte Radiator	
	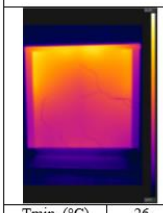		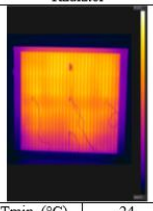		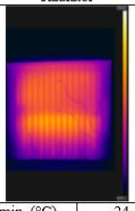	
	Tmin. (°C)	26	Tmin. (°C)	24	Tmin. (°C)	24
	Tmax. (°C)	83	Tmax. (°C)	81	Tmax. (°C)	124
60	Tave. (°C)	59	Tave. (°C)	64	Tave. (°C)	82
	Sample C, Oil-filled Panel Heater				Sample D, Electric Filament Heater	
	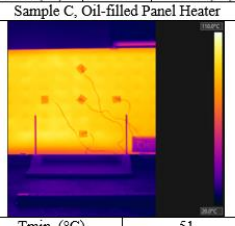				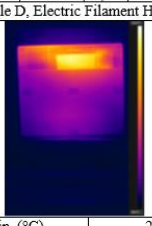	
	Tmin. (°C)	51			Tmin. (°C)	28
	Tmax. (°C)	102			Tmax. (°C)	122
	Tave. (°C)	92			Tave. (°C)	62

	Trust		Sample A, Fireclay Radiator		Sample B, Clay Chamotte Radiator	
	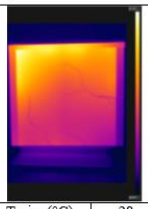		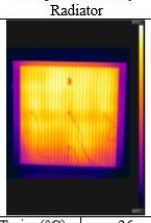		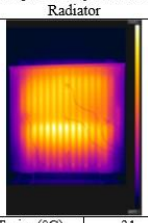	
	Tmin. (°C)	28	Tmin. (°C)	26	Tmin. (°C)	31
	Tmax. (°C)	91	Tmax. (°C)	91	Tmax. (°C)	153
T_{max}	Tave. (°C)	59	Tave. (°C)	70	Tave. (°C)	101
	Sample C, Oil-filled Panel Heater				Sample D, Electric Filament Heater	
	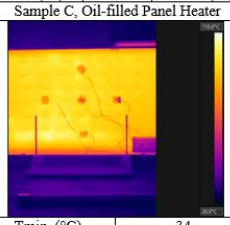				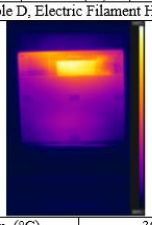	
	Tmin. (°C)	34			Tmin. (°C)	30
	Tmax. (°C)	106			Tmax. (°C)	124
	Tave. (°C)	93			Tave. (°C)	63

Table 2 depicts the temperature fields mentioned in table 1 but the temperature scale has been kept same for easy comparison. All samples are on the same scale from 20°C to 153°C. When observing all five samples it can be identified how the extent of temperature varies with respect to time. In the first 15 minutes, Sample C is seen to heat up significantly with the highest average front surface temperature of 72 °C against the other samples, aside from the filament exhibited in Sample D.

It is observed that the Trust sample predominantly has the coolest maximum average front surface temperature at 59°C through the heating cycle. After 30 minutes of heating, Sample A and Sample C show comparatively minimal variations as time progresses from 15 minutes of heating during the cycle. Sample D on the other hand, depicts comparatively negligible variations from 15 minutes of heating during the cycle and Sample B is seen to have the most variations in temperature as time increases during the heating cycle. This suggests, Sample D reaches its steady state in the shortest time whereas Sample B continues to increase past the tested heating cycle period. Further to this, it can be seen how the samples discharge heat in comparison to each other.

The Trust sample has its heat distribution towards the top of the sample, whereas the rest of the sample is relatively cooler towards the bottom. The Trust sample appears not to retain the heat within the carcass unlike the Samples A, B and C as the temperatures, here are significantly high. This suggests heat is discharged predominantly through radiation for these samples and through convection for Samples A and B. The heat distribution for Sample D is predominantly on the grill and the filament behind the grill, while the rest of the sample remains relatively cooler. The convection grills are on the front surface of the sample and can be observed to be allowing the heated air to discharge through these grills. The central bottom region and the area around the grill is warmer than the lower sides of the sample.

Table 3 shows the cooling cycle. This is an important part of testing as it signifies how long heat is retained in the sample core allowing it to be slowly discharged into the environment. If the heat up and cool down is fast then the thermal inertia is low, however, if the heat up and cool down is slow, then the

thermal inertia of the sample is high. For effective heating there needs to be a good balance in thermal inertia, such that the heat up is in reasonable time and the cool down is prolonged. Prolonged cool down means that the environment will remain in proximity of the desired temperature, making it cost-efficient as the sample will continue to emit heat without energy usage, hence without incurring cost.

Observing the cool down on independent scales of the samples show the rate at which each sample cool down with respect to time. All samples depict a reasonably uniform distribution of a temperature decrease across the front surface with respect to time.

It is noticed the Trust sample depicts an average temperature of 49°C after 15 minutes of cooling. This is a decrease of 10°C from its maximum average temperature in the heating cycle. In 60 minutes, the sample reaches an average temperature of 31°C, which is a further decrease of 18°C. There is more prominent heat dissipation occurring at the top half of the sample than the bottom half where temperature is relatively cooler. This is due to heat naturally flowing to the cooler area allowing a larger difference in temperature in the warmer region than the cooler region.

Table 2. Heating Cycle Comparative Analysis

Time (mins)	Thermography Data		
	Trust	Sample A, Fireclay Radiator	Sample B, Clay Chamotte Radiator
15	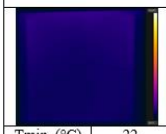	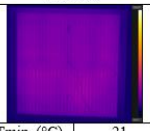	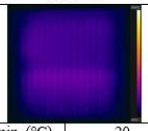
	Tmin. (°C) 22 Tmax. (°C) 43 Tave. (°C) 34	Tmin. (°C) 21 Tmax. (°C) 61 Tave. (°C) 46	Tmin. (°C) 20 Tmax. (°C) 58 Tave. (°C) 40
	Sample C, Oil-filled Panel Heater		Sample D, Electric Filament Heater
	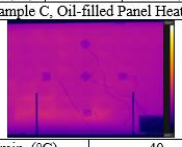		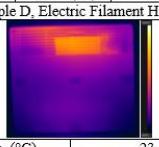
	Tmin. (°C) 40 Tmax. (°C) 85 Tave. (°C) 72		Tmin. (°C) 23 Tmax. (°C) 121 Tave. (°C) 60
30	Trust	Sample A, Fireclay Radiator	Sample B, Clay Chamotte Radiator
	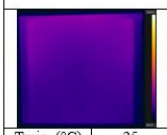	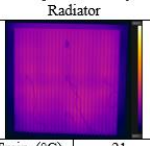	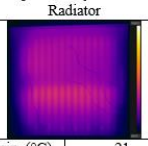
	Tmin. (°C) 25 Tmax. (°C) 65 Tave. (°C) 48	Tmin. (°C) 21 Tmax. (°C) 82 Tave. (°C) 63	Tmin. (°C) 21 Tmax. (°C) 89 Tave. (°C) 60
	Sample C, Oil-filled Panel Heater		Sample D, Electric Filament Heater
	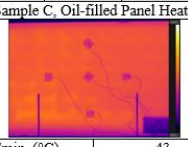		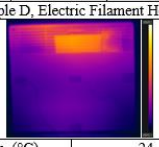
	Tmin. (°C) 43 Tmax. (°C) 110 Tave. (°C) 97		Tmin. (°C) 24 Tmax. (°C) 121 Tave. (°C) 61
60	Trust	Sample A, Fireclay Radiator	Sample B, Clay Chamotte Radiator
	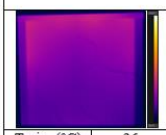	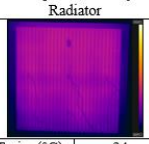	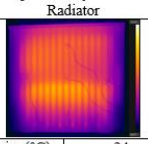
	Tmin. (°C) 26 Tmax. (°C) 83 Tave. (°C) 59	Tmin. (°C) 24 Tmax. (°C) 81 Tave. (°C) 64	Tmin. (°C) 24 Tmax. (°C) 124 Tave. (°C) 82
	Sample C, Oil-filled Panel Heater		Sample D, Electric Filament Heater
	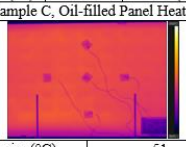		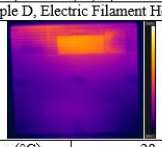
	Tmin. (°C) 51 Tmax. (°C) 102 Tave. (°C) 92		Tmin. (°C) 28 Tmax. (°C) 122 Tave. (°C) 62
T_{max}	Trust	Sample A, Fireclay Radiator	Sample B, Clay Chamotte Radiator
		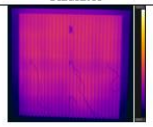	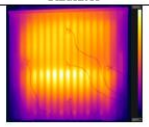
	Tmin. (°C) 28 Tmax. (°C) 91 Tave. (°C) 59	Tmin. (°C) 26 Tmax. (°C) 91 Tave. (°C) 70	Tmin. (°C) 31 Tmax. (°C) 153 Tave. (°C) 101
	Sample C, Oil-filled Panel Heater		Sample D, Electric Filament Heater
	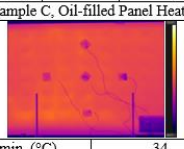		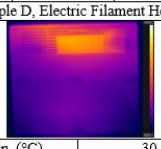
	Tmin. (°C) 34 Tmax. (°C) 106 Tave. (°C) 93		Tmin. (°C) 30 Tmax. (°C) 124 Tave. (°C) 63

Sample A is seen to cool down to 43°C in the first 15 minutes of its cooling cycle. This is a temperature decrease of 27°C from its maximum average temperature during its heating cycle. Similar to the Trust sample, Sample A depicts prominent heat dissipation from the top half of the sample than the bottom half. By the end of the 60-minute cooling period, the bottom half of the sample has reached the room temperature prior to beginning the experimentation of 20°C.

Sample B depicts a decreased average temperature by 18°C in the first 15 minutes of its cooling cycle. The sample cools down prominently from the top region of the bottom half as this is where the high temperature zones are exhibited. By the end of the cooling cycle, this sample reaches an average temperature of 32°C, which is the highest compared to the other samples.

Sample C depicts at decreased average temperature of 91°C at 15 minutes into its cool down cycle. This is a decrease of only 2°C from its maximum average temperature at the end of its heating cycle. It is noticed that in relation to 15 minutes of its cooling, the temperature decrease is not very prominent until after 30 minutes of cooling. This sample depicts a uniform temperature decrease distribution due to its oil-filled core.

Sample D is seen to decrease in temperature relatively quickly from an average temperature of 63°C to 28°C in the first 15 minutes of cooling. The average temperature decreases in a maximum increment of 3°C through the cycle and is seen to have uniform temperature distribution through the cooling cycle. It can however be seen that the filament behind the grills remains to be the highest temperature during this decrease and has a more significant fluctuations in temperature through the cooling cycle.

The cool down on the same scale in Table 4 depicts that Samples A and D cools down faster than the Trust sample throughout their cooling cycles, while Samples B and C cool down slower. However, by the end of the cooling cycle, there appears to be negligible difference between Trust and Sample C regarding their front surface temperatures. By the end of the cooling cycle, Sample A depicts the coolest front surface temperature in comparison with the other samples.

Observing how fast Sample D cools down after 15 minutes of cooling, it can be clearly seen, thermal inertia of a resistance convector heater is low. This means that the environment will quickly cool down after the heater is disabled and means it would not be very cost-efficient. The top sector of the bottom half of sample B depicts slightly higher temperature in this region in comparison with the other samples. It appears to cool down comparably slower than the other samples, however, the initial temperature at the end of its heating cycle was excessively high, therefore its is difficult to identify this sample as having a high thermal inertia.

Table 3. Cooling Cycle Independent Analysis

Time (mins)	Thermography Data					
	Trust		Sample A, Fireclay Radiator		Sample B, Clay Chamotte Radiator	
	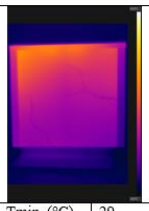		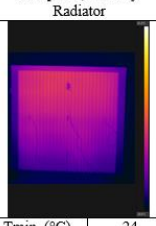		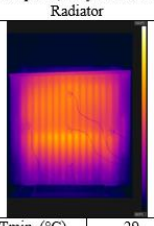	
15	Tmin. (°C) Tmax. (°C) Tave. (°C)	29 70 49	Tmin. (°C) Tmax. (°C) Tave. (°C)	24 57 43	Tmin. (°C) Tmax. (°C) Tave. (°C)	29 124 84
	Sample C, Oil-filled Panel Heater			Sample D, Electric Filament Heater		
	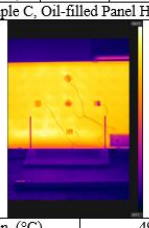			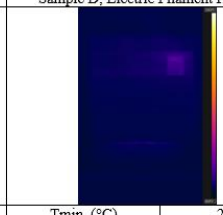		
	Tmin. (°C) Tmax. (°C) Tave. (°C)	49 103 91		Tmin. (°C) Tmax. (°C) Tave. (°C)	26 46 28	
	Trust		Sample A, Fireclay Radiator		Sample B, Clay Chamotte Radiator	
	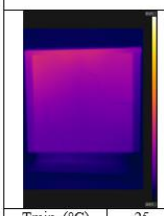		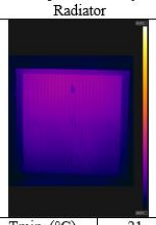		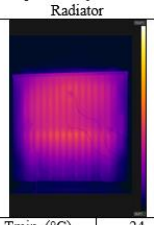	
30	Tmin. (°C) Tmax. (°C) Tave. (°C)	25 54 40	Tmin. (°C) Tmax. (°C) Tave. (°C)	21 45 35	Tmin. (°C) Tmax. (°C) Tave. (°C)	24 99 68
	Sample C, Oil-filled Panel Heater			Sample D, Electric Filament Heater		
	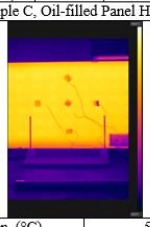			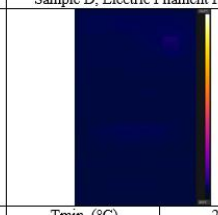		
	Tmin. (°C) Tmax. (°C) Tave. (°C)	51 97 90		Tmin. (°C) Tmax. (°C) Tave. (°C)	25 33 26	

	Trust		Sample A, Fireclay Radiator		Sample B, Clay Chamotte Radiator	
					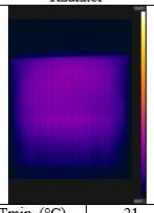	
60	Tmin. (°C) Tmax. (°C) Tave. (°C)	23 38 31	Tmin. (°C) Tmax. (°C) Tave. (°C)	20 32 27	Tmin. (°C) Tmax. (°C) Tave. (°C)	21 66 49
	Sample C, Oil-filled Panel Heater			Sample D, Electric Filament Heater		
				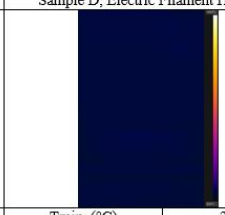		
	Tmin. (°C) Tmax. (°C) Tave. (°C)	32 49 43		Tmin. (°C) Tmax. (°C) Tave. (°C)	24 27 25	
	Trust		Sample A, Fireclay Radiator		Sample B, Clay Chamotte Radiator	
	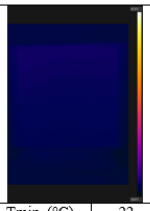				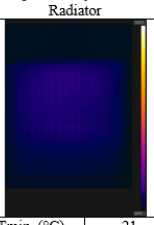	
T_{max}	Tmin. (°C) Tmax. (°C) Tave. (°C)	22 27 25	Tmin. (°C) Tmax. (°C) Tave. (°C)	20 24 22	Tmin. (°C) Tmax. (°C) Tave. (°C)	21 40 32
	Sample C, Oil-filled Panel Heater			Sample D, Electric Filament Heater		
	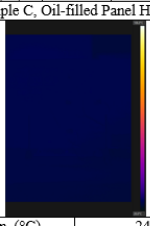			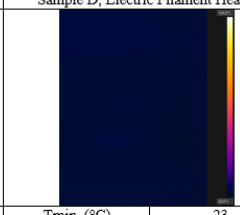		
	Tmin. (°C) Tmax. (°C) Tave. (°C)	24 27 25		Tmin. (°C) Tmax. (°C) Tave. (°C)	23 27 24	

From sample C it can be seen to have the minimal temperature difference of 2°C from the end of its heating cycle to 15 minutes into its cooling cycle in comparison with other samples. At 30 minutes of cooling, the average temperture is 90°C and at 60 minutes of cooling, the temperature decreases significantly to 43°C. This is a decrease of 27°C, which is the most significant decrease in average temperature from all the samples in this timeframe. Sample D has the most significant decrease in temperature of 35°C from the end of its heating cycle to 15 minutes into its cooling cycle from the rest of the samples. Aside from the filament situated behind the convector grills, the sample itself depicts the most uniform temperature distribution and temperature difference throughout the cooling cycle in comparison with the other samples.

Table 4. Cooling Cycle Comparative Analysis

Time (mins)	Thermography Data					
	Trust		Sample A, Fireclay Radiator		Sample B, Clay Chamotte Radiator	
	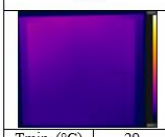		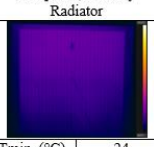		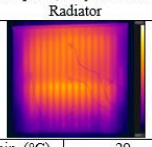	
	Tmin. (°C)	29	Tmin. (°C)	24	Tmin. (°C)	29
	Tmax. (°C)	70	Tmax. (°C)	57	Tmax. (°C)	124
15	Tave. (°C)	49	Tave. (°C)	43	Tave. (°C)	84
	Sample C, Oil-filled Panel Heater				Sample D, Electric Filament Heater	
	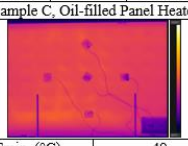				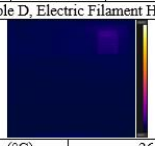	
	Tmin. (°C)	49			Tmin. (°C)	26
	Tmax. (°C)	103			Tmax. (°C)	46
	Tave. (°C)	91			Tave. (°C)	28
	Trust		Sample A, Fireclay Radiator		Sample B, Clay Chamotte Radiator	
	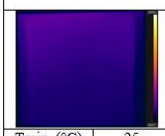		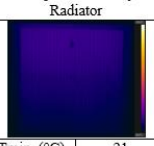		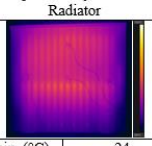	
	Tmin. (°C)	25	Tmin. (°C)	21	Tmin. (°C)	24
	Tmax. (°C)	54	Tmax. (°C)	45	Tmax. (°C)	99
30	Tave. (°C)	40	Tave. (°C)	35	Tave. (°C)	68
	Sample C, Oil-filled Panel Heater				Sample D, Electric Filament Heater	
	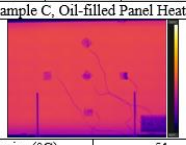				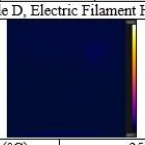	
	Tmin. (°C)	51			Tmin. (°C)	25
	Tmax. (°C)	97			Tmax. (°C)	33
	Tave. (°C)	90			Tave. (°C)	26
	Trust		Sample A, Fireclay Radiator		Sample B, Clay Chamotte Radiator	
	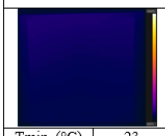		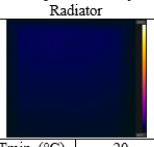		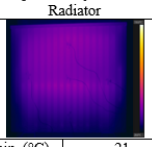	
	Tmin. (°C)	23	Tmin. (°C)	20	Tmin. (°C)	21
	Tmax. (°C)	38	Tmax. (°C)	32	Tmax. (°C)	66
60	Tave. (°C)	31	Tave. (°C)	27	Tave. (°C)	49
	Sample C, Oil-filled Panel Heater				Sample D, Electric Filament Heater	
	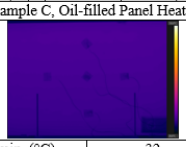				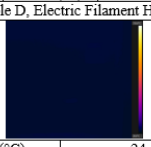	
	Tmin. (°C)	32			Tmin. (°C)	24
	Tmax. (°C)	49			Tmax. (°C)	27
	Tave. (°C)	43			Tave. (°C)	25
	Trust		Sample A, Fireclay Radiator		Sample B, Clay Chamotte Radiator	
			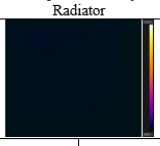		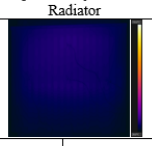	
	Tmin. (°C)	22	Tmin. (°C)	20	Tmin. (°C)	21
	Tmax. (°C)	27	Tmax. (°C)	24	Tmax. (°C)	40
T_{max}	Tave. (°C)	25	Tave. (°C)	22	Tave. (°C)	32
	Sample C, Oil-filled Panel Heater				Sample D, Electric Filament Heater	
	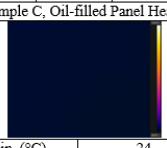				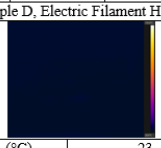	
	Tmin. (°C)	24			Tmin. (°C)	23
	Tmax. (°C)	27			Tmax. (°C)	27
	Tave. (°C)	25			Tave. (°C)	24

5.2. Thermocouple Measurements

Figure 10 depicts thermocouple measurements across the front radiator surface at the five locations illustrated in Figure 7, namely at (a) top; (b) left; (c) bottom; (d) left; (e) centre. The Trust sample exhibits the lowest front surface temperature on at the top and centre of the sample, while the radiator B exhibits the highest temperatures at the top, left, right and centre of the sample with a critically damped signal. The radiator D exhibits lowest temperature on the left and right of the sample. Both, the Trust sample, and the radiator D simultaneously show low temperatures at the bottom of the front radiator surface. This is due to the fluctuations in the Trust sample and the constant signal for the radiator D.

The radiator B exhibits prominent fluctuations in its signal throughout the cycle in all locations. This suggests the radiator reaches the desired room temperature, allowing the cut-off internal to the electric radiator to activate, slowly reducing the temperature for a certain amount of time. This in turn, saves both, electricity, and cost. The Trust sample has also been found to behave in a similar manner, though comparatively less prominent on the left.

The radiator C operates via radiant heat with its oil-filled core. It depicts an overshoot followed by some underdamping in its signal, suggesting the sample is constantly fluctuating in its energy usage. Further to this, it can be seen that the radiator D warms up in the shortest amount of time while the Trust sample takes the longest prior to reaching its steady state. The radiator B takes the longest amount of time to reach its steady state.

The radiator D exhibits low temperature on the front surface as it is a convector heater, meaning the heated air is discharged through the grill of the heater. This means heat is no longer retained and being an electric filament heater, it heats up instantly and cools down instantly when switched off. The disadvantage of this is that high concentration molecules in the air transfers into the low concentration regions and when the heater is switched off, there is no high concentration molecules being emitted. For this, since no heat is retained stored in the system, which slowly discharges, the environment is difficult to maintain the room temperature. The trend for the radiator D sample is seen to be steady and at a constant. This suggests that the sample is constantly using the same amount of electricity, which does not incur in any cost savings as the Trust sample and Competitor A sample would do.

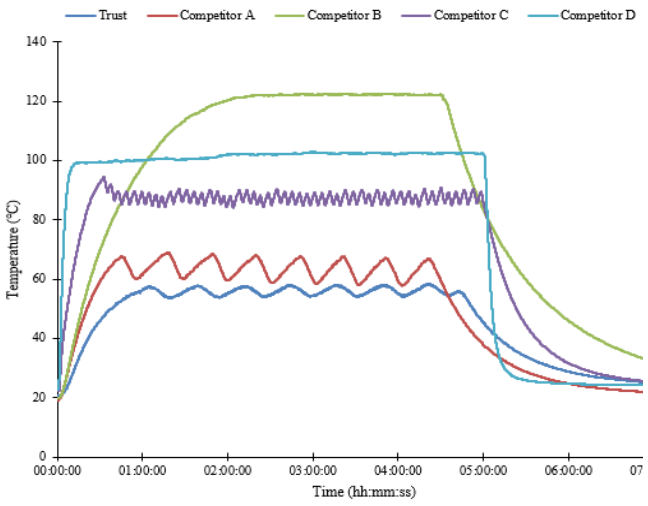

(a)

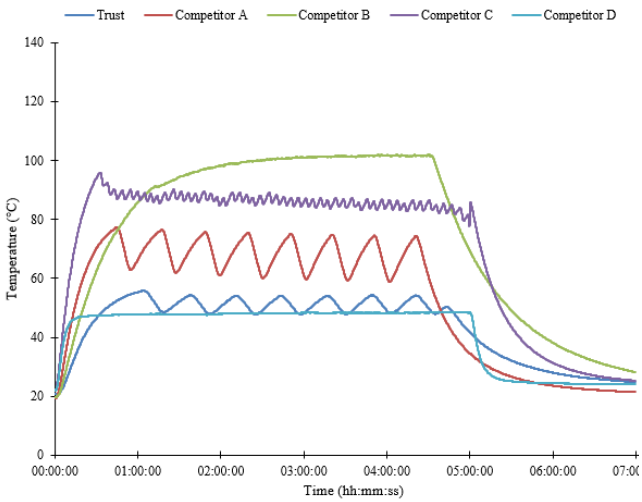

(b)

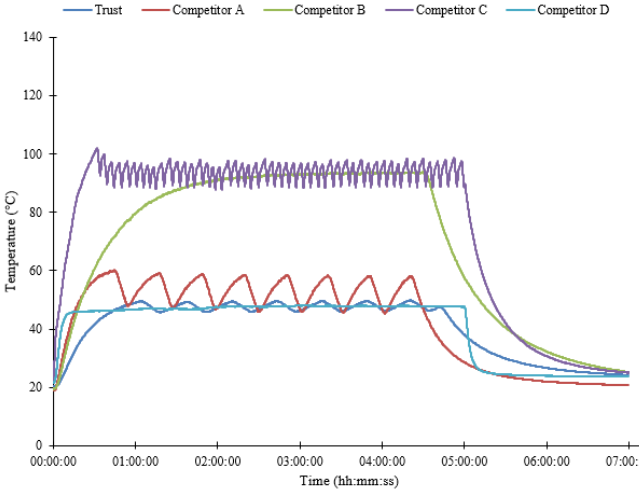

(c)

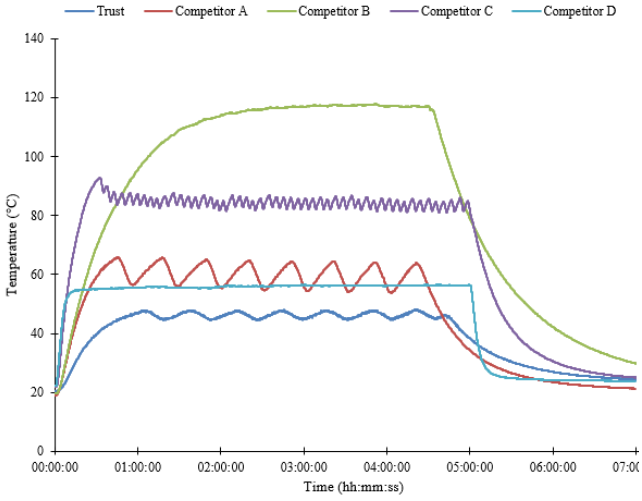

(d)

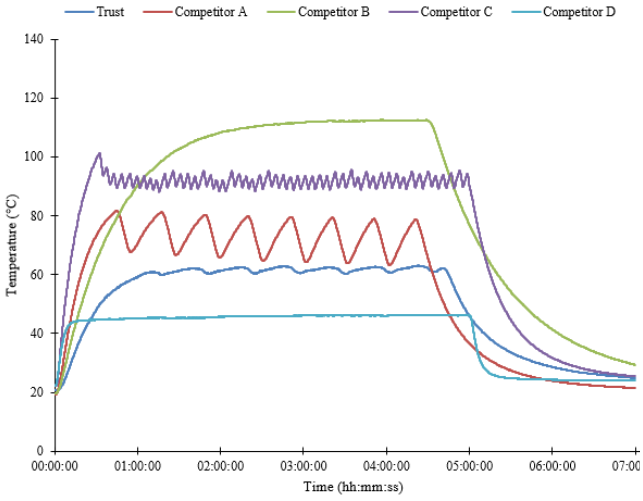

(e)

Figure 10: Thermocouple temperature variations at multiple locations on the front radiator surface (a) Location 1 - top (b) Location 2 - left (c) Location 3 - bottom (d) Location 4 - right and (e) Location 5 - centre

6. Conclusions

Thermal experimentations have been carried out to observe the thermal heat distribution of five heating solutions across its heating and cooling cycles. This data has been captured using an infrared thermal camera and thermocouples. Results depicted that the Trust sample had the coolest front surface temperature from all samples and its therefore comparably the safest sample out of the five. This further means a reduction in energy usage and hence lower running costs. It has also been discovered that the radiator C achieved the highest average temperature during its heating cycle in the first 15 minutes and the Trust sample was the slowest to warm up from the five samples, suggesting that the Trust radiator exhibits a greater level of convection than the other samples that appeared to be more radiant heaters.

During the cooling cycle, it has been found that the radiator A had the coolest front surface temperature at the end of its cycle and the radiator D cooled down the quickest. the radiator B was found to have cooled down the slowest, suggesting that it has the highest thermal inertia however, this sample exhibited excessively extreme high temperatures reaching beyond 100°C during its heating cycle and naturally be a responsible factor in the reasoning behind the slow cool down. while none of the heaters achieved the goal of lower than 43ºC to be classified as low a surface temperature (LST) heater, the Trust model came closest with highest surface temperature of 59ºC. It is hence considered the safest among the tested competing models for heating domestic and commercial dwellings. For future work to gain a clearer understanding of the effect of heater surface temperature on overall heating performance, and hence tie LST with performance, it is suggested that the comfort conditions of the environment should be investigated while specifying a desired room temperature.

7. References

[1] T. Fawcett and A. Hurst, “Carbon uk,” Oxford, 2002.

[2] J. A. Clarke, C. M. Johnstone, N. J. Kelly, P. A. Strachan, and P. Tuohy, "The role of built environment energy efficiency in a sustainable UK energy economy," *Energy Policy*, vol. 36, no. 12, pp. 4605–4609, Dec. 2008.

[3] B. Raybould, W. M. Cheung, C. Connor, and R. Butcher, "An investigation into UK government policy and legislation to renewable energy and greenhouse gas reduction commitments," *Clean Technol. Environ. Policy*, vol. 22, no. 2, pp. 371–387, Mar. 2020.

[4] T. Asim *et al.*, "Thermal characterization of commercial electric radiators," in *International Journal of COMADEM*, 2019, vol. 22, no. 2, pp. 27–31.

[5] V. A. Hemadri, A. Gupta, and S. Khandekar, "Thermal radiators with embedded pulsating heat pipes: Infra-red thermography and simulations," *Appl. Therm. Eng.*, vol. 31, no. 6–7, pp. 1332–1346, May 2011.

[6] T. Calisir, H. O. Yazar, and S. Baskaya, "Thermal performance of PCCP panel radiators for different convector dimensions – An experimental and numerical study," *Int. J. Therm. Sci.*, vol. 137, pp. 375–387, Mar. 2019.

[7] A. Taheri-Garavand *et al.*, "An intelligent approach for cooling radiator fault diagnosis based on infrared thermal image processing technique," *Appl. Therm. Eng.*, vol. 87, pp. 434–443, Aug. 2015.

[8] J. Wernik, M. Grabowski, and K. J. Wołosz, "Thermal Analysis of Radiator Under Natural and Forced Convection Conditions Using Numerical Simulation and Thermography," *Chem. Eng. Trans.*, vol. 70, 2018.

[9] M. Altwieb, K. J. Kubiak, A. M. Aliyu, and R. Mishra, "A new three-dimensional CFD model for efficiency optimisation of fluid-to-air multi-fin heat exchanger," *Therm. Sci. Eng. Prog.*, vol. 19, Oct. 2020.

[10] M. Altwieb, R. Mishra, A. M. Aliyu, and K. J. Kubiak, "Heat Transfer Enhancement by Perforated and Louvred Fin Heat Exchangers," *Energies*, vol. 15, no. 2, p. 400, Jan. 2022.

[11] A. M. Aliyu, D. Singh, C. Uzoka, and R. Mishra, "Dispersion of virus-laden droplets in ventilated rooms: Effect of homemade facemasks," *J. Build. Eng.*, vol. 44, p. 102933, Dec. 2021.

[12] Atcelec.co.uk, "Low Surface Temperature Radiators (LST) - ATC UK," 2019. [Online]. Available: https://atcelec.co.uk/low-surface-temperature-radiators-lst/. [Accessed: 15-Jan-2022].

[13] J. Vicarage, "WHAT ARE LOW SURFACE TEMPERATURE RADIATORS?," *Jaga Climate Designers*, 2022. [Online]. Available: https://jaga.co.uk/blog/what-are-low-surface-temperature-radiators. [Accessed: 15-Jan-2022].

[14] R. Mansell, "What Are LST Radiators?," *CounterHeating.co.uk*, 2021. [Online]. Available: https://www.contourheating.co.uk/blog/lst-radiators-explained. [Accessed: 15-Jan-2022].

[15] FLIR, "FLIR A655SC Datascheet." Teledyne FLIR LLC, 2019.